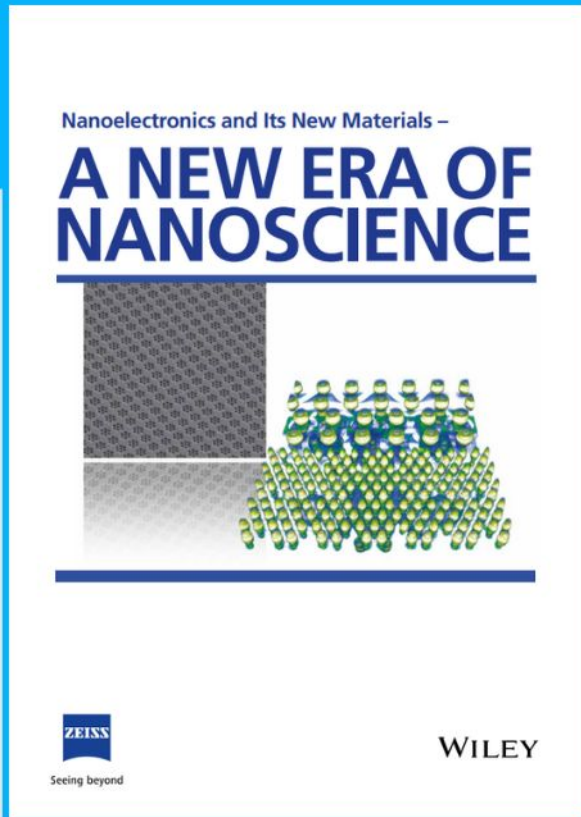




# Nanoelectronics and Its New Materials – A NEW ERA OF NANOSCIENCE



**Discover the recent advances in electronics research and fundamental nanoscience.**

Nanotechnology has become the driving force behind breakthroughs in engineering, materials science, physics, chemistry, and biological sciences. In this compendium, we delve into a wide range of novel applications that highlight recent advances in electronics research and fundamental nanoscience. From surface analysis and defect detection to tailored optical functionality and transparent nanowire electrodes, this eBook covers key topics that will revolutionize the future of electronics.

To get your hands on this valuable resource and unleash the power of nanotechnology, simply download the eBook now. Stay ahead of the curve and embrace the future of electronics with nanoscience as your guide.



Seeing beyond

**WILEY**

# Column-to-Beam Structure House Inspired MXene-Based Integrated Membrane with Stable Interlayer Spacing for Water Purification

Yanmei Zhang, Xushuai Chen, Chunjia Luo,\* Jincui Gu,\* Mengru Li, Min Chao, Xi Chen, Tao Chen, Luke Yan,\* and Xun Wang\*

$Ti_3C_2T_x$  (MXene) displays prominent properties in water purification due to its rich surface chemistry and physicochemical property. However, the separation property is severely restrained because of the intercalation-induced swelling. Inspired by the column-to-beam structure house, an advanced MXene-based membrane is developed with a stable interlayer spacing for water purification. Lamellar  $Ti_3C_2T_x$  nanosheets with numerous nanochannels are set as the “beam” part, and the boron nitride (BN) nanosheets are thought of as the “brick” part of the MXene-based integrated membrane. Moreover, the  $Ti_3C_2T_x$  nanosheets form stable interactions with the BN nanosheets through covalent cross-linking and supramolecular hydrogen bonding. Furthermore polydopamine and polyethylenimine assume the roles of the “column” part of this membrane through covalent cross-linking interaction. Therefore, this membrane shows outstanding anti-swelling property with a stable interlayer spacing of  $14.7 \pm 0.13 \text{ \AA}$  after 600 h immersion in water, which is superior to that of most previously reported works. In addition, its hydrophilic functional groups and charges endow itself with exceptional anti-fouling ability. This work may offer a promising manner to construct advanced separation materials with a stable structure for precise water purification.

scalability, high separation efficiency, and low energy consumption.<sup>[2]</sup> Especially, 2D membranes have become promising building blocks to control mass transport.<sup>[3]</sup> The ultrathin nanosheets of these membranes are stacked together to form a layer-to-layer structure.<sup>[4]</sup> Among these layers, numerous channels are created among the neighboring nanosheets, serving as selective channels to realize ultimate separation efficiency. To date, several 2D membranes have been established, such as  $Ti_3C_2T_x$  (MXene),<sup>[5]</sup> boron nitride (BN),<sup>[6]</sup> graphene oxide (GO),<sup>[7]</sup> graphite phase carbon nitride ( $g-C_3N_4$ ),<sup>[8]</sup> covalent organic frameworks (COF),<sup>[9]</sup> molybdenum disulfide ( $MoS_2$ ),<sup>[10]</sup> and metal-organic framework (MOF) nanosheets.<sup>[11]</sup>

As a young 2D material, MXene is of enormous interest in diverse fields attributing to its unique physicochemical property and rich surface chemistry.<sup>[12]</sup> On the one hand, MXene has numerous terminations on the surface, including =O, –OH, and –F, owing to the aqueous medium, which is beneficial for subsequent chemical functionalization.<sup>[3c,13]</sup> On the other hand, its interlayer space can be controlled for selective molecular separation.<sup>[14]</sup> Besides, the MXene-based membranes possessed other excellent characteristics, such as mechanical flexibility and thermal stability.<sup>[2c,15]</sup> In addition, previous works demonstrated that the  $Ti_3C_2T_x$  nanosheets with a large

## 1. Introduction

Water scarcity is a global issue worldwide resulting from climate change, contamination of freshwater resources, and population growth.<sup>[1]</sup> Toward this crisis, membrane separation technology has become a competitive candidate for treating contaminated wastewater due to its superiorities, including


–OH, and –F, owing to the aqueous medium, which is beneficial for subsequent chemical functionalization.<sup>[3c,13]</sup> On the other hand, its interlayer space can be controlled for selective molecular separation.<sup>[14]</sup> Besides, the MXene-based membranes possessed other excellent characteristics, such as mechanical flexibility and thermal stability.<sup>[2c,15]</sup> In addition, previous works demonstrated that the  $Ti_3C_2T_x$  nanosheets with a large

Y. M. Zhang, X. S. Chen, C. J. Luo, M. R. Li, M. Chao, X. Chen, T. Chen, L. K. Yan  
Polymer Materials and Engineering Department  
School of Materials Science and Engineering  
Chang'an University  
Xi'an 710064, China  
E-mail: luochunjia@chd.edu.cn; yanlk\_79@hotmail.com

J. C. Gu, T. Chen  
Key Laboratory of Marine Materials and Related Technologies  
Zhejiang Key Laboratory of Marine Materials and Protective Technologies  
Ningbo Institute of Material Technology and Engineering  
Chinese Academy of Science  
Ningbo 315201, China  
E-mail: gujincui@nimte.ac.cn

J. C. Gu, T. Chen  
School of Chemical Sciences  
University of Chinese Academy of Science  
Beijing 100049, China

X. Wang  
Department of Chemistry  
Key Lab of Organic Optoelectronics and Molecular Engineering  
Tsinghua University  
Beijing 100084, China  
E-mail: wangxun@mail.tsinghua.edu.cn

 The ORCID identification number(s) for the author(s) of this article can be found under <https://doi.org/10.1002/adfm.202111660>.

DOI: 10.1002/adfm.202111660

aspect ratio could bring the regular interlayer space, leading to a good separation efficiency with slight flux loss.<sup>[16]</sup> Hence, MXene is an essential candidate for developing 2D membranes for water purification. However, the water molecules can be spontaneously absorbed into the interlayer space of the MXene nanosheets, resulting in swelling and poor stability.<sup>[12a,17]</sup> Therefore, exploiting effective means to construct advanced MXene-based membranes with stable structures is highly required.

Fortunately, the abundant surface terminations of the MXene make it possible to tune the interlayer spacing of the  $Ti_3C_2T_x$  nanosheets to suppress their swelling in the aqueous environment.<sup>[12a,18]</sup> So far, several alternative strategies have been taken to address the swelling issues for water purification. Wang et al. fabricated the MXene-based membranes by self-cross-linking reaction and  $Al^{3+}$  ions intercalation, successively. In the former work, the Ti–O–Ti bonds among the neighboring MXene nanosheets can endow this membrane with anti-swelling property with stable interlayer spacing at  $\approx 15.4$  Å.<sup>[19]</sup> Therefore, this membrane presented a good anti-swelling property during 70 h of long-term ion separation. In the latter work, the strong interaction between the  $Al^{3+}$  and MXene prevented the swelling of MXene and kept its interlayer spacing at  $15.1 \pm 0.2$  Å for up to 400 h.<sup>[14]</sup> Jin et al. prepared the MXene-based membrane with an interlayer spacing of  $\approx 15.5$  Å for efficient solvent dehydration through interfacial polymerization. This membrane exhibited good separation performance for water/isopropanol mixtures.<sup>[20]</sup> Wang et al. fabricated the

MXene membrane with a stabilizing interlayer spacing of  $16.2 \pm 0.2$  Å through using the alginate hydrogel. This membrane presented excellent separation properties toward valent cations.<sup>[21]</sup> Wang et al. prepared a laminated MXene-based membrane with regular slit-shaped nanochannels to separate antibiotics in water and/or organic solvents.<sup>[16]</sup> Liu et al. fabricated an MXene-based membrane with tunable lamellar nanochannels by self-assembling  $Ti_3C_2T_x$  nanosheets and alumina nanoparticles. This membrane demonstrated stability separation performance after 20 h of filtration.<sup>[22]</sup> Despite these advances, developing a facile strategy to construct the MXene-based membrane with a more stable interlayer spacing for water purification is highly desired.

In the construction field, the column-to-beam structure house is usually built to improve its earthquake resistance capacity. Inspired by this, we demonstrated a new methodology to construct an MXene-based laminar membrane with stable interlayer spacing through alternating 2D–2D assembly and covalent molecular cross-linking reaction (Figure 1). Specifically, the  $Ti_3C_2T_x$  (MXene) nanosheets were acted as the “beam” part, and the boron nitride (BN) nanosheets were thought of as the “brick” part of the MXene-based integrated membrane. The  $Ti_3C_2T_x$  nanosheets and BN nanosheets were assembled into the 2D/2D architecture by cross-linking reaction and supramolecular hydrogen bonding, which can restrict the swelling of the MXene membrane (Figure 1a,b).<sup>[4b]</sup> Moreover, the polydopamine (PDA) and polyethylenimine (PEI) assumed the role of the “column”

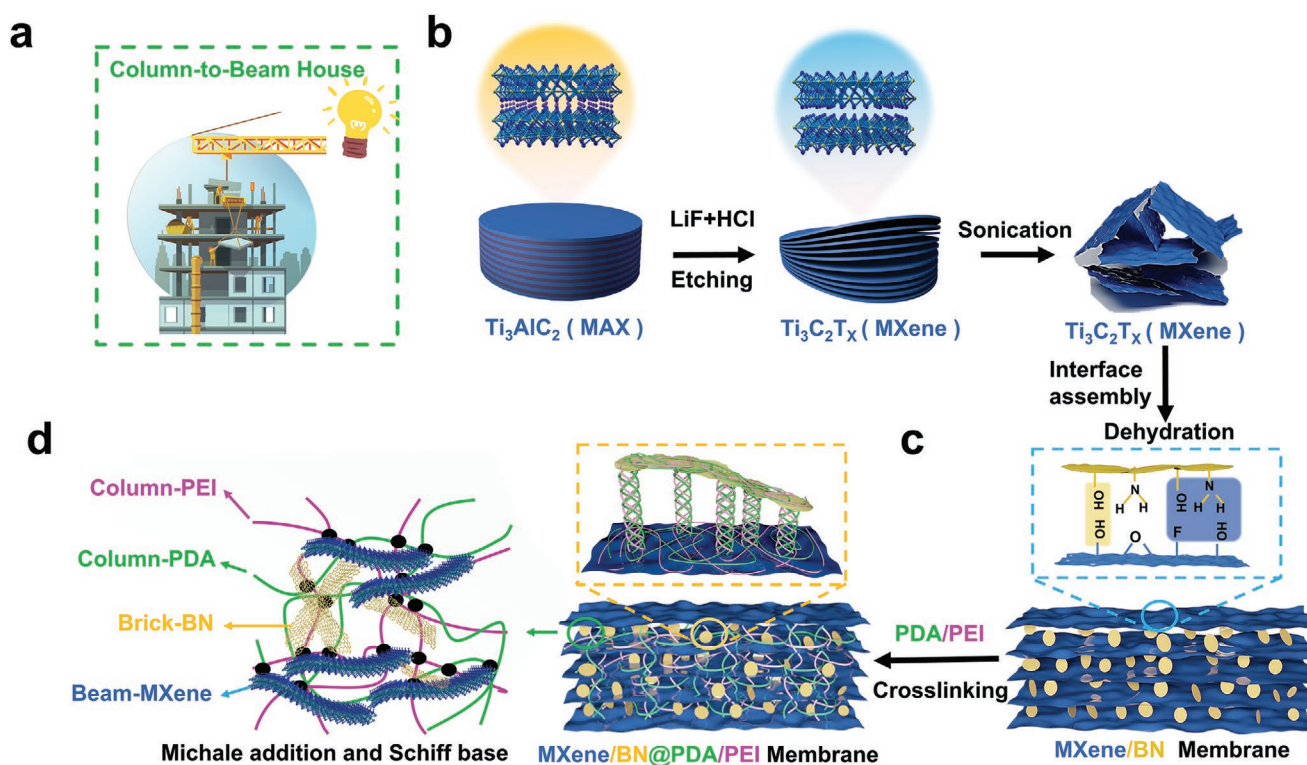


**Figure 1.** Schematic illustration of the fabrication process of the MXene/BN@PDA/PEI membrane for water purification. a) The house with the column-to-beam structure. b) The  $Ti_3AlC_2$  (MAX) was etched with  $LiF$  and  $HCl$  to fabricate the  $Ti_3C_2T_x$  (MXene) nanosheets. c) The  $Ti_3C_2T_x$  (MXene) acted as the “beam” part, and BN nanosheets were thought of as the “brick” part. They were assembled into the 2D/2D architecture by cross-linking reaction and hydrogen bonding. d) The PDA and PEI assumed the role of the “column” part of the MXene/BN@PDA/PEI membrane through the covalent cross-linking reaction.

part through the covalent cross-linking reaction to endow the MXene/BN@PDA/PEI membrane with the interlayer spacing of  $14.7 \pm 0.13 \text{ \AA}$  (Figure 1c). Inspiringly, the MXene/BN@PDA/PEI membrane kept its initial interlayer spacing even after the 600 h swelling test, indicating its excellent anti-swelling property (Figure 1d). In addition, the hydrophilic functional groups and abundant charges endowed this membrane with excellent anti-fouling ability. This work introduced a facile route to construct an MXene-based membrane with a more stable interlayer spacing to satisfy water purification requirements.

## 2. Results and Discussion

The layered precursors  $\text{Ti}_3\text{AlC}_2$  (MAX) were etched with the LiF-HCl mixing solution to remove the Al element selectively and thereby got the  $\text{Ti}_3\text{C}_2\text{T}_x$  (MXene) nanosheets.<sup>[23,24]</sup> X-ray diffraction (XRD) was used to study the crystallinity of the  $\text{Ti}_3\text{C}_2\text{T}_x$  (MXene) nanosheets and  $\text{Ti}_3\text{AlC}_2$  (MAX). As shown in Figure 2a, the intense diffraction peak at  $39.10^\circ$  (104) in the  $\text{Ti}_3\text{AlC}_2$  (MAX) disappeared, and the (002) peak shifted left in the XRD pattern indicating the selective removal of Al in the  $\text{Ti}_3\text{AlC}_2$  (MAX) phase.<sup>[14,24a]</sup> Moreover, scanning electron microscopy (SEM) was carried out to survey the micromorphology of the  $\text{Ti}_3\text{C}_2\text{T}_x$

(MXene) nanosheets. The  $\text{Ti}_3\text{C}_2\text{T}_x$  (MXene) nanosheets were split from each other like an accordion-like structure, indicating the successful etching of the  $\text{Ti}_3\text{AlC}_2$  (MAX) (Figure 2b and Figure S1, Supporting Information). The lateral size of the  $\text{Ti}_3\text{C}_2\text{T}_x$  (MXene) was  $\approx 1.5 \mu\text{m}$  (Figure 2c). The transmission electron microscopy (TEM) and atomic force microscopy (AFM) image revealed that the  $\text{Ti}_3\text{C}_2\text{T}_x$  (MXene) nanosheets were thin and almost transparent (Figure S2, Supporting Information). Their average thickness was  $\approx 1.36 \text{ nm}$ , and there were almost no structural defects (Figure 2c). The high aspect ratio of the  $\text{Ti}_3\text{C}_2\text{T}_x$  (MXene) nanosheets reduced the meso- and macropores' presence and ensured the uniformity of the MXene-based membranes.<sup>[16]</sup>

The microstructure of the BN nanosheets was also characterized through SEM and TEM. Figure 2d showed that the BN nanosheet presented an ellipse-shaped feature, and its edge was smooth (Figure S3, Supporting Information). Its thickness was  $\approx 7.8 \text{ nm}$ , and the average lateral size was  $\approx 252 \text{ nm}$ , which was smaller than that of the  $\text{Ti}_3\text{C}_2\text{T}_x$  (MXene) nanosheets (Figure 2e). The MXene/BN membrane was obtained through the vacuum-assisted interface assembly. The MXene/BN membrane was rougher than the MXene membrane (Figure 2f,g). The thickness of the MXene/BN membrane was  $5.90 \pm 0.24 \mu\text{m}$  (Figure 2h and Figure S4, Supporting Information). The

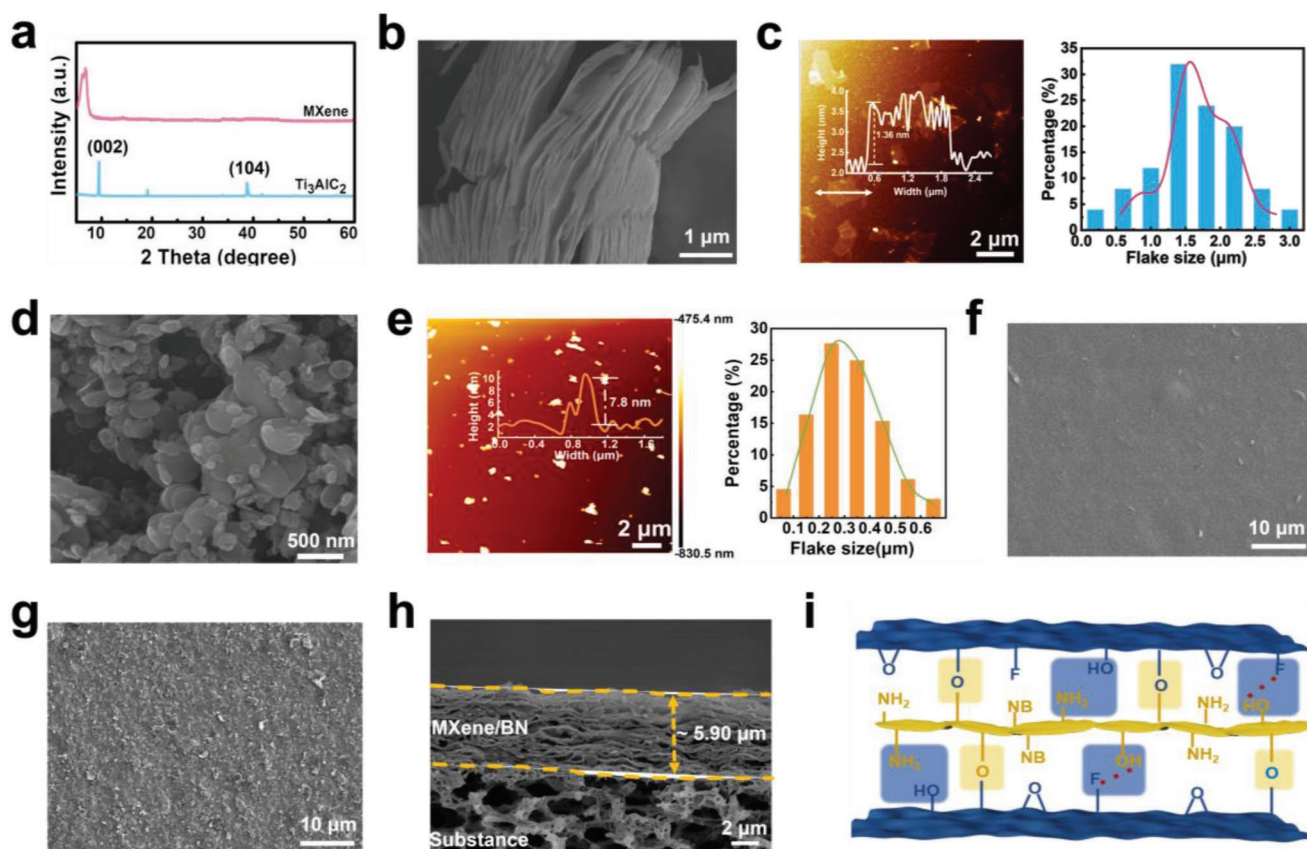


**Figure 2.** a) XRD patterns of the  $\text{Ti}_3\text{AlC}_2$  (MAX) powder and  $\text{Ti}_3\text{C}_2\text{T}_x$  (MXene) nanosheets. b) SEM image of the  $\text{Ti}_3\text{C}_2\text{T}_x$  (MXene) nanosheets. c) AFM image of the  $\text{Ti}_3\text{C}_2\text{T}_x$  (MXene) nanosheets (left) and its corresponding size distribution (right). Inset: the thickness height of the  $\text{Ti}_3\text{C}_2\text{T}_x$  (MXene) nanosheet. d) SEM image of the BN nanosheets. e) AFM image of the BN nanosheets (left) and its corresponding size distribution (right). Inset: the thickness height of the BN nanosheets. SEM images of the f) MXene membrane and g) MXene/BN membrane. h) SEM image of the cross-section of the MXene/BN membrane. i) Schematic diagram of the interaction between the MXene nanosheets and BN nanosheets.

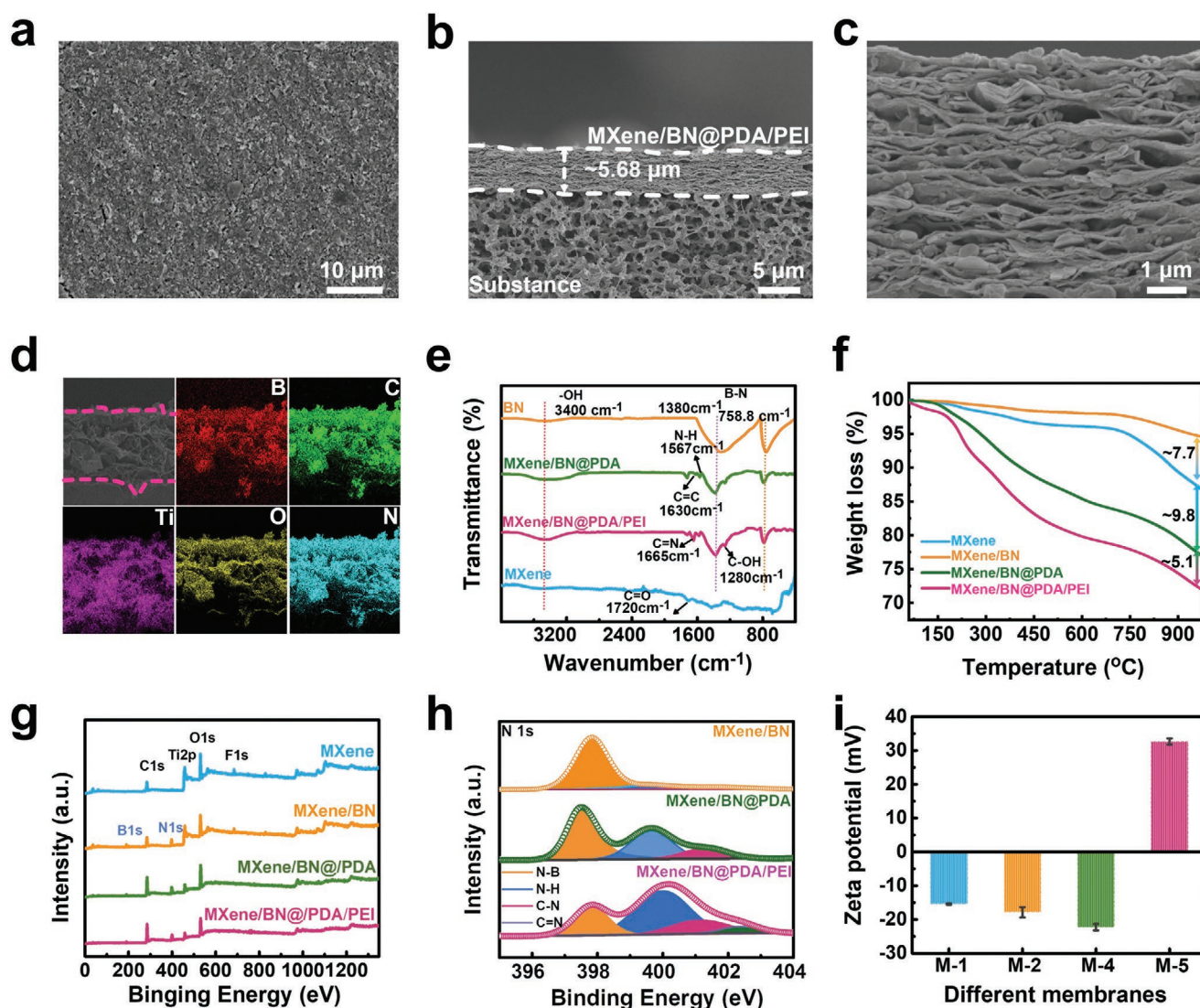


**Figure 3.** a) SEM image of the MXene/BN@PDA/PEI membrane. b,c) SEM image of a cross-section of the MXene/BN@PDA/PEI membrane and its responding enlarged image. d) EDS elemental maps of the MXene/BN@PDA/PEI membrane. e) FTIR spectra of the MXene membrane, BN membrane, MXene/BN@PDA membrane, and MXene/BN@PDA/PEI membrane. f) TGA results of the MXene membrane, MXene/BN membrane, MXene/BN@PDA membrane, and MXene/BN@PDA/PEI membrane. g) XPS spectra of the MXene membrane, MXene/BN membrane, MXene/BN@PDA membrane, and MXene/BN@PDA/PEI membrane. h) N 1s XPS spectra with the fitting results of the MXene/BN membrane, MXene/BN@PDA membrane, and MXene/BN@PDA/PEI membrane. i) Zeta potential of the (M-1) MXene membrane, (M-2) MXene/BN membrane, (M-4) MXene/BN@PDA membrane, and (M-5) MXene/BN@PDA/PEI membrane.

$\text{Ti}_3\text{C}_2\text{T}_x$  nanosheets were stacked in a well-aligned manner with BN nanosheets through dehydration and supramolecular hydrogen bonding due to the high aspect ratio (Figure 2i). The  $\text{Ti}_3\text{C}_2\text{T}_x$  nanosheets provided the main transport channel due to their large lateral dimensions, and BN nanosheets achieved hybridization intercalation while filling edge defects or voids.

SEM was further carried out to characterize the micromorphology of the MXene/BN@PDA/PEI membrane. As shown in Figure 3a, the MXene/BN@PDA/PEI membrane was rougher than the MXene membrane. The cross-sectional SEM image in Figure 3b,c showed that the MXene/BN@PDA/PEI membrane firmly adhered to the substrate. These nanosheets were well stacked to form a laminate column-to-beam structure with the

thickness of  $5.68 \pm 0.19 \mu\text{m}$ , which was slightly higher than the MXene/BN@PDA membrane ( $5.34 \pm 0.52 \mu\text{m}$ ) and MXene/BN@PEI membrane ( $5.51 \pm 0.33 \mu\text{m}$ ) (Figure S4, Supporting Information).

Furthermore, energy dispersive spectroscopy (EDS) results distinctly illustrated the homogeneous distribution of the C, O, Ti, B, and N elements in the MXene/BN@PDA/PEI membrane (Figure 3d). Fourier-transform infrared spectroscopy (FTIR) was further performed to study the chemical composition of the MXene/BN@PDA/PEI membrane. As shown in Figure 3e, the broad absorption peak at  $\approx 3400 \text{ cm}^{-1}$  was assigned to the  $-\text{OH}$  vibration peak. The absorption peak at  $\approx 1720 \text{ cm}^{-1}$  was assigned to the  $-\text{C}=\text{O}$  peak in the MXene membrane.<sup>[20]</sup> The sharp absorption peak at  $\approx 1380$  and  $\approx 758 \text{ cm}^{-1}$  were representatives of

the stretching vibration and the bending vibration of the B–N bond, indicating the successful modification of BN nanosheets on the MXene membrane.<sup>[24]</sup> In addition, the absorption peak at  $\approx 1280$  and  $\approx 1630$   $\text{cm}^{-1}$  represented the stretching vibration of the phenolic hydroxyl group and benzene ring of PDA. Moreover, the absorption peak at  $\approx 1567$   $\text{cm}^{-1}$  was the N–H stretching vibration in the PDA and PEI. The new peak at  $\approx 1665$   $\text{cm}^{-1}$  was the C=N stretching vibration by the Schiff base cross-linking reaction of the PEI and PDA molecules.

Besides, from the thermogravimetric analysis (TGA) results, the thermal stability of the MXene membrane could be improved due to the presence of BN sheets.<sup>[25]</sup> In addition, there were  $\approx 17.5\%$  and  $\approx 5.1\%$  mass losses, indicating the functionalization of the PDA and PEI (Figure 3f). These results firmly demonstrated the successful functionalization of different components on the MXene membrane. The chemical characterization of these membranes was also analyzed by X-ray photoelectron spectroscopy (XPS). As presented in Figure 3g, O 1s ( $\approx 530$  eV), C 1s ( $\approx 285$  eV), and Ti 2p ( $\approx 458$  eV) appeared in all the membranes. The C 1s spectrum could be decomposed into four peaks at 288.21, 285.75, 284.07, and 281.12 eV, which was assigned to C=O, C–O, C–C, and –C–Ti, respectively (Figure S5a, Supporting Information).<sup>[20,26]</sup> Moreover, the O 1s spectrum could be divided into three peaks at 529.41, 530.87, and 532.38 eV, which were assigned to –O–Ti–, –O–Ti–OH, and –O–C–OH,<sup>[26,27]</sup> respectively (Figure S5b, Supporting Information). Furthermore, N 1s ( $\approx 399$  eV) and B 1s ( $\approx 191$  eV) emerge in the MXene/BN membrane after modifying BN nanosheets.<sup>[26]</sup> There were four peaks in the N 1s spectrum, including –N–B, –N–H, –C–N, –C=N at around 397.24, 399.13, 400.53, and 401.64 eV, respectively (Figure 3h).<sup>[28]</sup> It was worth noting that the N content in the MXene/BN@PDA/PEI membrane increased from  $\approx 10.84\%$  to  $\approx 13.38\%$  compared to the MXene/BN membrane, further proving the modification of PDA and PEI (Table S1–S4, Supporting Information).

Zeta potential was further carried out to test the stability and charge of different membranes. As shown in Figure 3i, the MXene membrane, MXene/BN membrane, and MXene/BN@PDA membrane presented a negative charge. In contrast, the MXene/BN@PDA/PEI membrane took on a positive charge, indicating the modification of PEI molecules. Moreover, the charge values of the MXene/BN@PDA/PEI membrane ( $33.7 \pm 0.9$  mV) was larger than that of the MXene membrane ( $-15.4 \pm 0.2$  mV), MXene/BN membrane ( $-178 \pm 1.5$  mV), and MXene/BN@PDA membrane ( $-22.3 \pm 0.8$  mV), indicating the MXene/BN membrane became more stable after the modification of PDA and PEI molecules. During the preparation process, the PDA, with abundant functionalized groups, such as hydroxyl and amine, can serve as the molecular linkers between PEI and MXene/BN through noncovalent interactions, including hydrogen bonding and charge transfer interactions (Figure S6, Supporting Information).<sup>[29]</sup> In addition, AFM was applied to characterize the fine microstructure of these membranes. As shown in Figure 4a–c, the MXene/BN@PDA/PEI membrane with the roughness of  $40.1 \pm 4.82$  nm was rougher than the MXene membrane ( $29.3 \pm 1.37$  nm).<sup>[30]</sup> Moreover, the MXene/BN@PDA/PEI membrane was smoother than the MXene/BN membrane ( $125.6 \pm 9.01$  nm), MXene/BN@PEI membrane

( $65.9 \pm 10.83$  nm), and MXene/BN@PDA membrane ( $86.1 \pm 20.11$  nm) (Figure S7, Supporting Information).

Besides, their responding surface wettability was investigated using the water contact angle (WCA). As shown in Figure 4d, the MXene membrane was hydrophilic with the WCA of  $81.00 \pm 1.0^\circ$  because of the oxygen-containing functionalities. Moreover, after the BN nanosheets assembly, the roughness and the content of oxygen-containing functionalities increased. According to Wenzel mode, the WCA of the MXene/BN membrane reduced to  $69.3 \pm 0.38^\circ$ . Besides, the MXene/BN@PDA, MXene/BN@PEI, and MXene/BN@PDA/PEI membranes were more hydrophilic with the WCA of  $34.93 \pm 0.91^\circ$ ,  $42.3 \pm 2.52^\circ$ , and  $11.66 \pm 0.57^\circ$ , respectively. The water droplet passed through the MXene/BN@PDA/PEI membrane within  $\approx 5$  s, which was faster than that of the MXene membrane ( $\approx 194$  s), MXene/BN membrane ( $\approx 61$  s), MXene/BN@PEI membrane ( $\approx 38$  s), and MXene/BN@PDA membrane ( $\approx 12$  s) (Movies S1–S5, Supporting Information). These results indicated the successful functionalization of different ingredients on the MXene/BN@PDA/PEI membrane.

Furthermore, the MXene/BN@PDA/PEI membrane showed underwater superoleophobicity with all the investigated oil contact angles above  $150^\circ$ , higher than the other membranes (Figure 4e,f). The MXene/BN@PDA/PEI membrane was infiltrated with water, and a continuous water layer was formed, resulting in blocking effective contact between oil and membrane surface. The oil droplet was rapidly detached from the MXene/BN@PDA/PEI membrane if it contacted its surface, mainly due to its interface morphology and chemical composition (Figure 4g,h).

The anti-swelling property of the MXene-based membranes was studied via XRD analysis. These membranes were immersed in deionized (DI) to ensure complete penetration of the water molecules. For the pristine MXene membrane, the (002) peak was located near  $6.7975^\circ$ , and the Bragg equation calculated the interlayer spacing to be  $13.05 \pm 0.04$  Å (Figures 4i and 5a).<sup>[23a]</sup> Due to the swelling property, the interlayer spacing of the original MXene membrane increased to  $16.44 \pm 0.07$  Å after the swelling test, which was consistent with previous literature.<sup>[21,23]</sup> For the MXene/BN membrane, its interlayer spacing increased from  $14.11 \pm 0.08$  to  $16.09 \pm 0.17$  Å, indicating the slightly suppressed swelling resulting from the neighboring  $\text{Ti}_3\text{C}_2\text{T}_x$  (MXene) nanosheets and BN nanosheets. In contrast, the MXene/BN@PDA membrane and MXene/BN@PEI membrane displayed smaller interlayer spacing shifted from  $13.82 \pm 0.07$  to  $15.35 \pm 0.05$  Å, and from  $13.96 \pm 0.07$  to  $15.59 \pm 0.09$  Å, respectively, indicating the interface functionalization of the PDA and PEI molecules.

Furthermore, it can be noted that the interlayer spacing of the MXene/BN@PDA/PEI membrane varied in a narrow range of 1.3 Å and was rigidly stabilized at  $14.7 \pm 0.13$  Å. These results suggested that the MXene/BN@PDA/PEI membrane exhibited a narrow 2D nanochannel structure and excellent anti-swelling property attributing to the Schiff/Michael addition reaction of the PDA and PEI molecules.<sup>[31]</sup> Besides, after continuous immersing for 600 h, the MXene/BN@PDA/PEI membrane has a more stable interlayer spacing than the MXene membrane (Figure 5b). In addition, a series of swelling property experiments were carried out to prove the stability

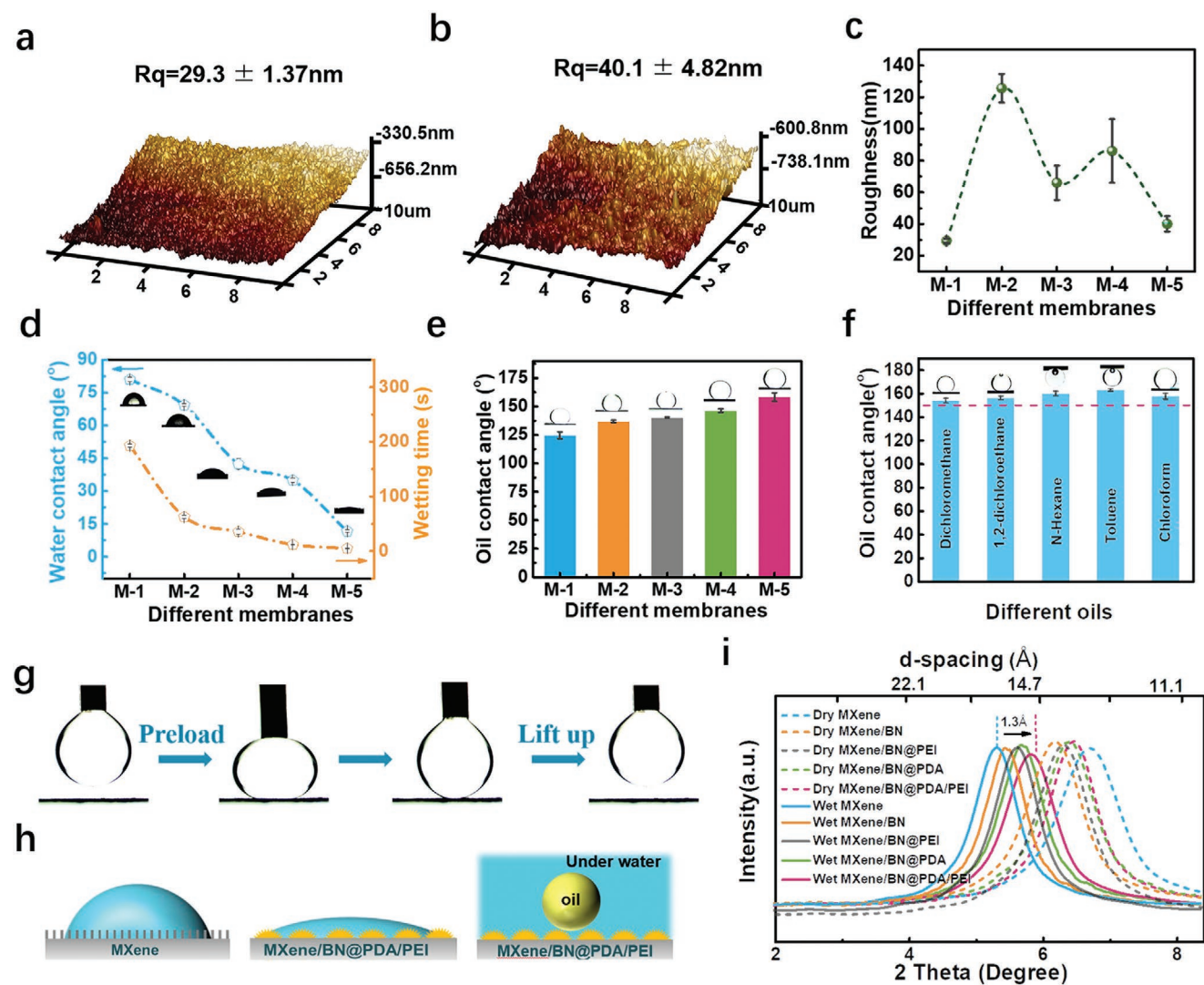


**Figure 4.** a) AFM image of the MXene membrane. b) AFM image of the MXene/BN@PDA/PEI membrane. c) The roughness of different membranes (M-1, MXene membrane; M-2, MXene/BN membrane; M-3, MXene/BN@PEI membrane; M-4, MXene/BN@PDA membrane; M-5, MXene/BN@PDA/PEI membrane). d) Water contact angle and wetting time of different membranes. e) The underwater oil contact angle of different membranes. f) The underwater oil contact of the MXene/BN@PDA/PEI membrane for various oils. g) The oil adhesion on the MXene/BN@PDA/PEI membrane underwater. h) Schematic illustration of the wettability of the MXene/BN@PDA/PEI membrane in air and underwater. i) XRD patterns of the MXene membrane, MXene/BN membrane, MXene/BN@PDA membrane, MXene/BN@PEI membrane, and MXene/BN@PDA/PEI membrane in different states.

of the MXene/BN@PDA/PEI membrane. Compared with the MXene membrane, the MXene/BN@PDA/PEI membrane kept its initial morphology and cross-sectional structure after being immersed in water for 600 h, indicating the stable lamellar structure of the MXene/BN@PDA/PEI membrane (Figure 5c–e and Figure S8, Supporting Information).

The unique wettability and anti-swelling properties made the MXene/BN@PDA/PEI membrane an ideal choice for water purification. This work set chloroform-in-water (C/W) emulsion as the representative oil-in-water emulsion (O/W) to evaluate its separation performance. The preparation process was optimized to obtain the MXene/BN@PDA/PEI composite membrane with excellent separation performance. First, we studied the effect of the mass ratio of the  $\text{Ti}_3\text{C}_2\text{T}_x$  (MXene) nanosheets and BN nanosheets on separation performance for C/W emulsion.

As shown in Figure 6a, the MXene/BN@PDA/PEI composite membrane showed a weak separation efficiency with a low  $\text{Ti}_3\text{C}_2\text{T}_x$  (MXene) nanosheets content. In contrast, it has a smaller separation flux when the content of  $\text{Ti}_3\text{C}_2\text{T}_x$  (MXene) and BN increased to 2:1 due to the large size of the  $\text{Ti}_3\text{C}_2\text{T}_x$  (MXene) nanosheets and the tortuous transmission route. To balance the “trade-off” between efficiency and flux, the optimal ratio of the  $\text{Ti}_3\text{C}_2\text{T}_x$  (MXene) nanosheets and BN nanosheets was 1:1. In this case, the separation flux of the MXene/BN@PDA/PEI membrane was  $143.63 \pm 6.85 \text{ L m}^{-2} \text{ h}^{-1} \text{ bar}^{-1}$  with an efficiency of  $99.5 \pm 0.4\%$ . Second, the effect of load capacity on its separation performance for C/W emulsion was discussed. It was found that the efficiency of the MXene/BN@PDA/PEI membrane gradually increased with the increase of the capacity load (Figure 6b,c). An excessive amount of MXene/BN@PDA/PEI

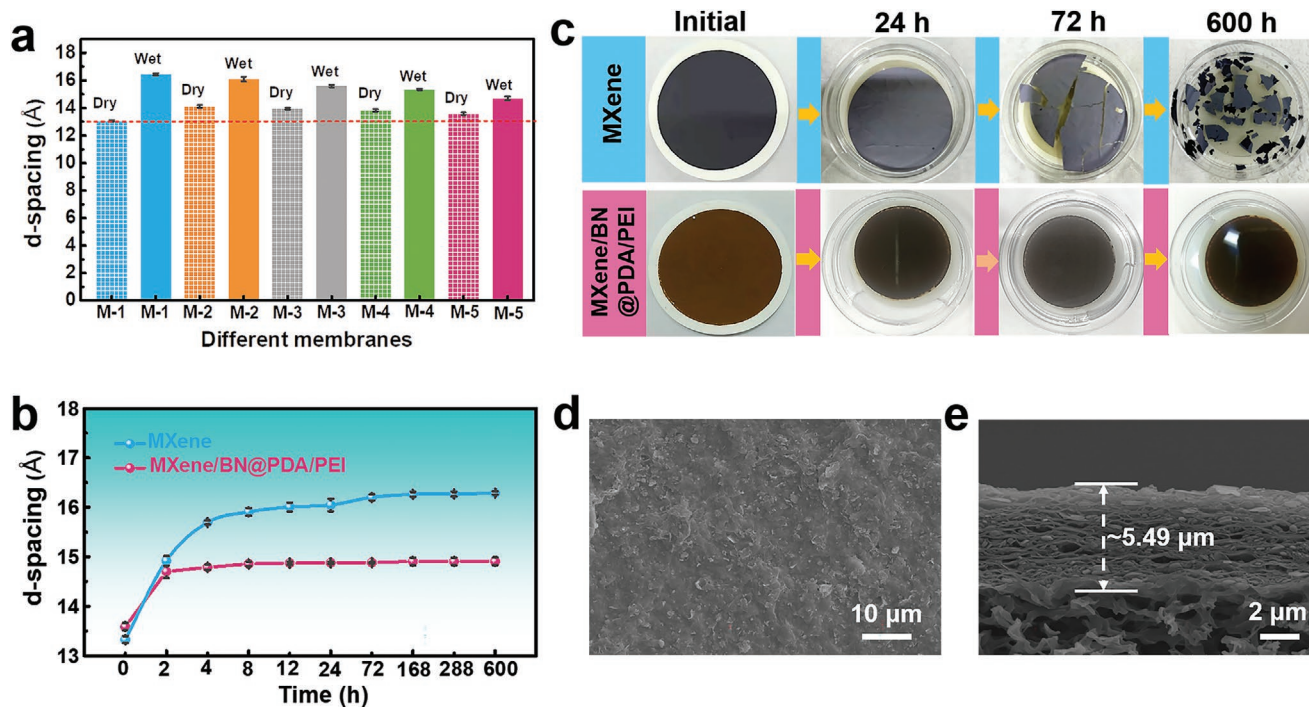


**Figure 5.** a) Interlayer spacing of the different membranes in different states (M-1, MXene membrane; M-2, MXene/BN membrane; M-3, MXene/BN@PEI membrane; M-4, MXene/BN@PDA membrane; M-5, MXene/BN@PDA/PEI membrane). b) Interlayer spacing results of the MXene/BN@PDA/PEI membrane with different immersing times. c) Photographs of the MXene membrane and MXene/BN@PDA/PEI membrane before and after being immersed in water for 600 h. d) SEM image of the MXene/BN@PDA/PEI membrane after immersing in water for 600 h. e) Cross-section SEM image of the MXene/BN@PDA/PEI membrane after immersing for 600 h.

caused the separation flux to drop sharply due to the increased thickness (Figure 6b,c and Figure S9, Supporting Information). Finally, the effect of cross-linking time on separation capacity was investigated. As shown in Figure 6d, the MXene/BN@PDA/PEI membrane presented an excellent separation performance when the cross-linking time was 0.5 h. The apparent change was due to the differentiated thickness of the MXene/BN@PDA/PEI membrane. The PDA and PEI molecules constantly penetrated the interior of the  $\text{Ti}_3\text{C}_2\text{T}_x$  (MXene) nanosheets. As shown in Figure S10, Supporting Information, the thickness of the MXene/BN@PDA/PEI membrane increased along with the prolonged cross-linking time of the PEI molecule. Too short cross-linking time led to insufficient structure, higher separation flux, and lower separation efficiency. However, too long cross-linking time resulted in the heavy accumulation of  $\text{Ti}_3\text{C}_2\text{T}_x$  nanosheets and lower separation flux.<sup>[32]</sup>

Based on these explorations, the separation performance of the MXene/BN@PDA/PEI membrane for various O/W emulsions was systematically studied. As shown in Figure 6e, the separation flux of the MXene/BN@PDA/PEI membrane for the 1,2-dichloroethane-in-water (Dc/W) emulsion, dichloromethane-in-water (Dm/W) emulsion, hexane-in-water (H/W) emulsion, C/W emulsion, and toluene-in-water (T/W) emulsion was  $95.76 \pm 5.75$ ,  $326.43 \pm 8.13$ ,  $874.96 \pm 18.47$ ,  $143.93 \pm 6.41$ , and  $77.53 \pm 1.91 \text{ L m}^{-2} \text{ h}^{-1} \text{ bar}^{-1}$ , respectively. The filtration was transported with the size distribution of  $\approx 1\text{--}100 \text{ nm}$  with the efficiency of  $96.54 \pm 0.91\%$ ,  $98.83 \pm 0.57\%$ ,  $94.90 \pm 2.09\%$ ,  $95.50 \pm 0.43\%$ , and  $96.46 \pm 0.15\%$ , respectively

(Figures S11–S13, Supporting Information). The separation performance of the MXene/BN@PDA/PEI membrane was superior to that of the other compared membranes (Figure 6e and Figure S4f, Supporting Information). The excellent performance of the MXene/BN@PDA/PEI membrane was due to the synergy of charge effect and hydration effect (Figure S14, Supporting Information).<sup>[33]</sup>

Furthermore, the MXene/BN@PDA/PEI membrane showed stable separation efficiency and flux for the C/W emulsion even after 45 cycles of separation (Figure 6f,g), indicating its excellent anti-fouling property. Besides, this membrane kept its initial separation performance even after 600 h of swelling test in an aqueous solution (Figure 6h,i). On the contrary, the separation efficiency of the MXene membrane, MXene/BN membrane, MXene/BN@PEI membrane, and MXene/BN@PDA membrane decreased from  $85.36 \pm 1.05\%$ ,  $88.43 \pm 1.89\%$ ,  $93.3 \pm 2.33\%$ ,  $96.8 \pm 0.26\%$  to  $73.38 \pm 2.04\%$ ,  $82.26 \pm 0.40\%$ ,  $87.7 \pm 0.17\%$ , and  $93.36 \pm 0.98\%$ , respectively (Figure 6h). In addition, even after 45 cycles of C/W emulsion separation, the interlayer spacing of the MXene/BN@PDA/PEI membrane was  $14.6 \pm 0.11 \text{ \AA}$ , which was almost consistent with that of the MXene/BN@PDA/PEI membrane with an interlayer spacing of  $14.7 \pm 0.13 \text{ \AA}$  (Figure 7a,b). More importantly, the MXene/BN@PDA/PEI membrane showed narrower and more stable interlayer spacing than most MXene-based membranes previously reported (Figure 7c and Table S5, Supporting Information). In addition, this membrane displayed stable separation performance even treatment under harsh conditions (Figure S15,



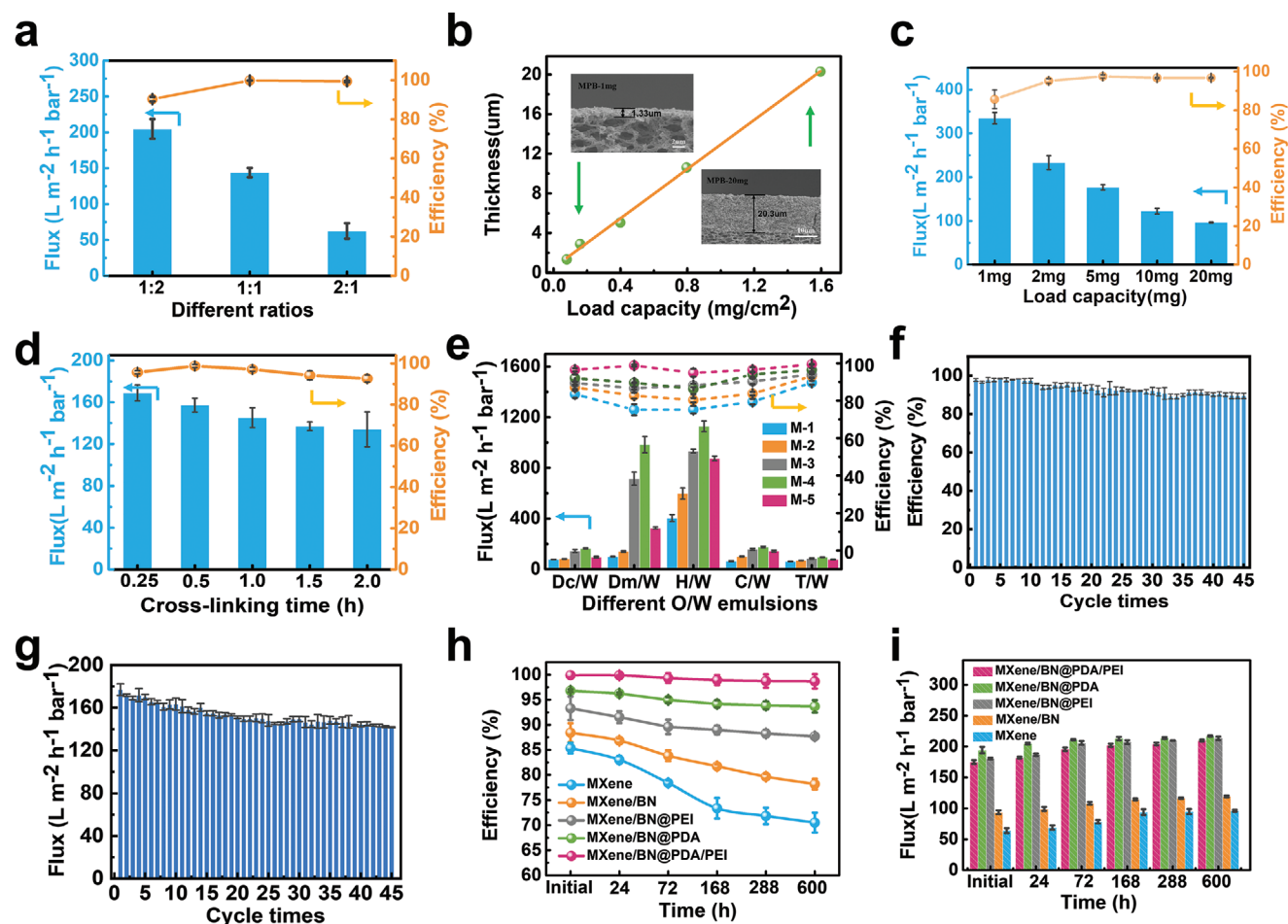


**Figure 6.** a) Separation performance of the MXene/BN@PDA/PEI membrane for C/W emulsion with different mass ratios of  $Ti_3C_2T_x$  (MXene) and BN. b) The linear relationship between loading and thickness of MXene/BN@PDA/PEI membrane. c) C/W emulsion separation performance of the MXene/BN@PDA/PEI membrane with different load capacities. d) Separation ability of the MXene/BN@PDA/PEI membrane with different cross-linking times of PEI molecules. e) Separation performance of MXene membrane (M-1), MXene/BN membrane (M-2), MXene/BN@PEI membrane (M-3), MXene/BN@PDA membrane (M-4), and MXene/BN@PDA/PEI membrane (M-5) for different O/W emulsions. f) Recycling separation efficiency and g) flux of the MXene/BN@PDA/PEI membrane for C/W emulsion. h, i) Separation efficiency and flux of different membranes for C/W emulsion after being immersed in water for 600 h.

Supporting Information). Besides, this membrane kept its initial interlayer spacing after treatment with strong acid or alkali solution, indicating its excellent environmental stability (Figure 7d). Furthermore, even after 45 cycles of separation, this membrane still maintained its initial surface structure and cross-sectional topography (Figure 7e,f), further demonstrating the stable nanochannel structure of the MXene/BN@PDA/PEI membrane and its excellent anti-swelling property.

### 3. Conclusion

MXene attracts extensive interest due to its numerous terminations, adjustable transmission channels, large aspect ratio, and so forth. However, the intercalation-induced swelling made the separation performance below the theoretical prediction. Inspired by architecture, an advanced MXene/BN@PDA/PEI membrane was constructed through the interface

assembly and subsequent functional modification to address this issue. The MXene/BN@PDA/PEI membrane showed superior anti-swelling property attributing to the lay-by-lay assembly of the  $Ti_3C_2T_x$  (MXene) and BN nanosheets and the cross-linking reaction of the PDA and PEI molecules. Excitingly, the interlayer spacing of this membrane was kept at  $14.7 \pm 0.13 \text{ \AA}$  after 600 h immersed in water, which was superior to the majority of the previous reports. Moreover, the MXene/BN@PDA/PEI membrane presented superhydrophilicity and has abundant positive charges. Besides, this membrane showed an excellent anti-fouling property under the synergy of hydration and charge effect. Therefore, this membrane displayed superior separation performance for O/W emulsion compared to other membranes. All these features make this membrane a good candidate for water purification. This work will offer new solutions for novel 2D membranes with excellent anti-swelling performance for wastewater purification.

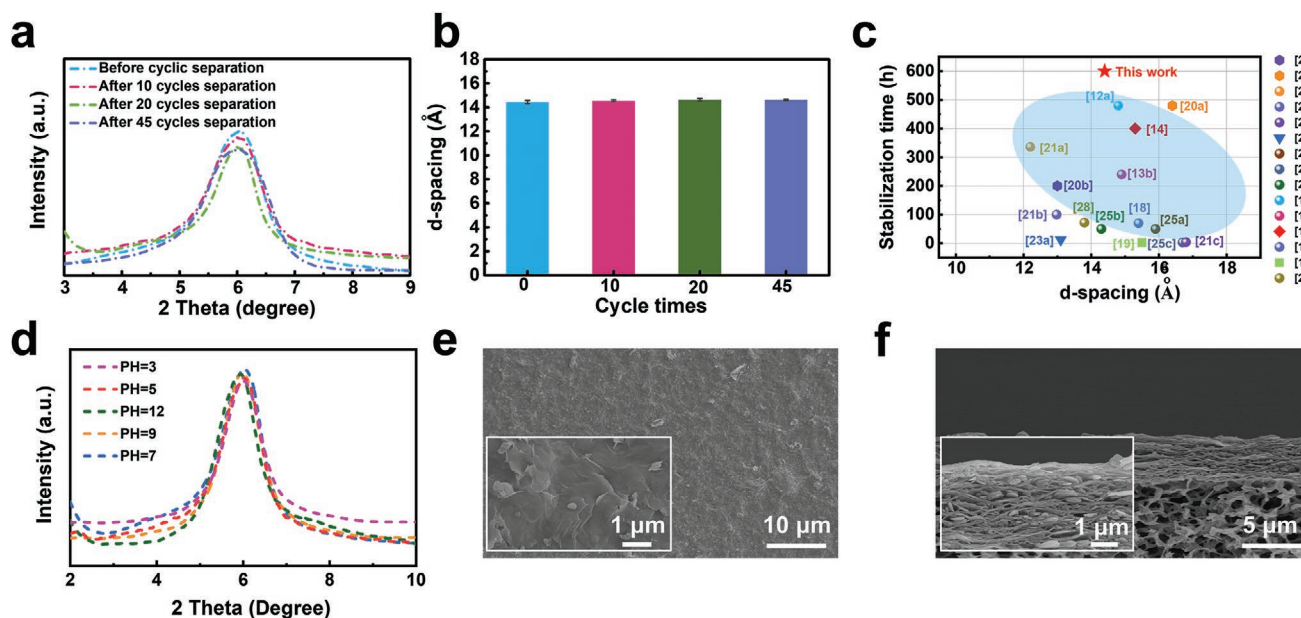


**Figure 7.** a) XRD patterns of the MXene/BN@PDA/PEI membrane before and after cyclic separation. b) The interlayer spacing results of the MXene/BN@PDA/PEI membrane before and after cyclic separation. c) The interlayer spacing and stabilization time comparison of different MXene-based membranes previous works and this work. d) XRD patterns of the MXene/BN@PDA/PEI composite membrane under different harsh environments for 6 days. e) SEM image and its magnified image of the MXene/BN@PDA/PEI membrane after 45 times cyclic separations. f) The cross-section and magnified SEM images of the MXene/BN@PDA/PEI membrane after 45 times cycle separation.

## Supporting Information

Supporting Information is available from the Wiley Online Library or from the author.

## Acknowledgements

The authors gratefully acknowledge funding from the National Natural Science Foundation of China (22005039), the Shaanxi Key Research and Development Project (2020ZDLGY13-08), Shaanxi Key Research and Development Project (2021GY199), Natural Science Basic Research Plan in Shaanxi Province of China (2021)Q-224), Public Welfare Science and Technology Projects of Ningbo (2021S150), Special Fund for Basic Scientific Research of Central Colleges, Chang'an University (300102319306, 300102312403), and K. C. Wong Education Foundation (G)TD-2019-13).

## Conflict of Interest

The authors declare no conflict of interest.

## Data Availability Statement

The data that support the findings of this study are available from the corresponding author upon reasonable request.

## Keywords

anti-fouling, anti-swelling, interlayer spacing, MXene, water purification

Received: November 16, 2021

Revised: January 30, 2022

Published online: February 23, 2022

- a) L. Nia, K. L. Goh, Y. Wang, J. Lee, Y. J. Huang, H. E. Karahan, K. Zhou, M. D. Guiver, T. H. Bae, *Sci. Adv.* **2020**, *6*, 9184;
  - b) Y. Q. Zhang, X. Q. Cheng, X. Jiang, J. J. Urban, C. H. Lau, S. Q. Liu, L. Shao, *Mater. Today* **2020**, *36*, 40;
  - c) J. Ge, H. Y. Zhao, H. W. Zhu, J. Huang, L. A. Shi, S. H. Yu, *Adv. Mater.* **2018**, *28*, 10459.
- a) J. C. Zhang, L. F. Liu, Y. Si, J. Y. Yu, B. Ding, *Adv. Funct. Mater.* **2020**, *30*, 25;
  - b) X. You, H. Wu, R. Zhang, Y. Su, L. Cao, Q. Yu, J. Yuan, K. Xiao, M. He, Z. Jiang, *Nat. Commun.* **2019**, *10*, 435;
  - c) H. E. Karahan, K. Goh, C. F. Zhang, E. Yang, C. Yildirim, C. Y. Chuah, M. G. Ahunbay, J. Lee, S. B. Tantekin-Ersolmaz, Y. Chen, T. H. Bae, *Adv. Mater.* **2020**, *32*, 1906697;
  - d) Y. Kang, Y. Xia, H. T. Wang, X. W. Zhang, *Adv. Funct. Mater.* **2019**, *29*, 1902014;
  - e) X. Lu, U. R. Cabinet, C. L. Ritt, X. Feng, A. Deshmukh, K. Kawabata, M. Kaneda, S. M. Hashmi, C. O. Osuji, M. Elimelech, *Environ. Sci. Technol.* **2020**, *54*, 9640;
  - f) B. Sapkota, W. Liang, A. VahidMohammadi, R. Karnik, A. Noy, M. Wanunu, *Nat. Commun.* **2020**, *11*, 2747.
- a) Y. Cai, D. Chen, N. Li, Q. Xu, H. Li, J. He, J. Lu, *Adv. Mater.* **2020**, *32*, 2001265;
  - b) Y. B. Yang, X. D. Yang, L. Liang, Y. Y. Gao, H. Y. Cheng, X. M. Li, M. C. Zou, R. Z. Ma, Q. Yuan, X. F. Duan, *Science* **2019**, *364*, 1057;
  - c) G. Liu, W. Jin, N. Xu, *Angew. Chem., Int. Ed.* **2016**, *55*, 13384;
  - d) E. Hoenig, S. E. Strong, M. Z. Wang, J. M. Radhakrishnan, N. J. Zaluzec, J. L. Skinner, C. Liu, *Nano. Lett.* **2020**, *20*, 7844.
- a) J. Y. Xia, P. Xiao, J. C. Gu, T. Y. Chen, C. H. Liu, L. K. Yan, T. Chen, *J. Mater. Chem. A* **2020**, *8*, 18735;
  - b) X. Feng, Z. Yu, R. Long, Y. Sun, M. Wang, X. Li, G. Zeng, *Sep. Purif. Technol.* **2020**, *247*, 117409.
- a) S. Anwer, D. H. Anjum, S. H. Luo, Y. Abbas, B. S. Li, S. Iqbal, K. Liao, *Chem. Eng. J.* **2021**, *406*, 126827;
  - b) X. Wu, M. M. Ding, H. Xu, W. Yang, K. S. Zhang, H. L. Tian, H. T. Wang, Z. L. Xie, *ACS Nano* **2020**, *14*, 9125;
  - c) A. Lipatov, H. D. Lu, M. Alhabeab, B. Anasori, A. Gruverman, Y. Gogotsi, A. Sinitski, *Sci. Adv.* **2018**, *4*, 0491.
- a) S. Qin, D. Liu, G. Wang, D. Portehault, C. J. Garvey, Y. Gogotsi, W. W. Lei, Y. Chen, *J. Am. Chem. Soc.* **2017**, *139*, 6314;
  - b) Z. Liu, A. Dibaji, D. Li, S. Mateti, J. Q. Liu, F. H. Yan, C. J. Barrow, Y. Chen, K. Ariga, W. R. Yang, *Mater. Today* **2021**, *44*, 194.

- [7] a) T. Wu, Z. Wang, Y. X. Lu, S. Liu, H. P. Li, G. Ye, J. Chen, *Adv. Sci.* **2021**, *8*, 2002717; b) L. Shen, Q. Shi, S. P. Zhang, J. Gao, D. C. Cheng, M. Yi, R. Y. Song, L. D. Wang, J. W. Jiang, R. Karnik, S. Zhang, *Sci. Adv.* **2021**, *7*, 6263.
- [8] a) L. T. Ji, L. K. Yan, M. Chao, M. R. Li, J. C. Gu, M. Lei, Y. M. Zhang, X. Wang, J. Y. Xia, T. Y. Chen, T. Y. Nia, T. Chen, *Small* **2021**, *17*, 2007122; b) Y. Wang, B. Y. Gao, Q. Y. Yue, Z. N. Wang, *J. Mater. Chem. A* **2020**, *8*, 19133; c) Y. N. Liu, Y. L. Su, J. Y. Guan, J. L. Cao, R. N. Zhang, M. R. He, K. Gao, L. J. Zhou, Z. Y. Jiang, *Adv. Funct. Mater.* **2018**, *28*, 1706546; d) F. He, B. C. Zhu, B. Cheng, J. G. Yu, W. K. Ho, W. Macyk, *Appl. Catal. B.* **2020**, *272*, 119006.
- [9] a) L. Yang, K. Meghdad, G. Y. Nan, D. Nan, S. Vahid, J. H. Long, *Matter* **2021**, *4*, 2590; b) F. Haase, B. V. Lotsch, *Chem. Soc. Rev.* **2020**, *49*, 8469; c) X. J. Zhao, P. Pachfule, A. Thomas, *Chem. Soc. Rev.* **2021**, *50*, 6871; d) H. W. Fan, M. H. Peng, I. Strauss, A. Mundstock, H. Meng, J. Caro, *J. Am. Chem. Soc.* **2020**, *142*, 6872.
- [10] a) W. Hirunpinyopas, E. Prestat, S. D. Worrall, S. J. Haigh, R. A. W. Dryfe, M. A. Bissett, *ACS Nano* **2017**, *11*, 11082; b) D. Ghim, Q. S. Jiang, S. S. Cao, S. Singamaneni, Y. S. Jun, *Nano Energy* **2018**, *53*, 949.
- [11] a) G. D. Wu, H. L. Zhou, Z. H. Fu, W. H. Li, J. W. Xiu, M. S. Yao, Q. H. Li, G. Xu, *Angew. Chem., Int. Ed.* **2021**, *60*, 9931; b) Y. Z. Li, Z. H. Fu, G. Xu, *Coord. Chem. Rev.* **2019**, *388*, 79.
- [12] a) D. D. Shao, Q. X. Zhang, L. Wang, Z. Y. Wang, Y. X. Jing, X. L. Cao, F. Zhang, S. P. Sun, *J. Membr. Sci.* **2021**, *623*, 119033; b) M. Naguib, M. Kurtoglu, V. Presser, J. Lu, J. J. Niu, M. Heon, L. Hultman, Y. Gogotsi, M. W. Barsoum, *Adv. Mater.* **2011**, *23*, 4248.
- [13] a) J. Shen, G. Z. Liu, Y. F. Ji, Q. Liu, L. Cheng, K. C. Guan, M. C. Zhang, G. P. Liu, J. Xiong, J. Yang, W. Q. Jin, *Adv. Funct. Mater.* **2018**, *28*, 1801511; b) S. C. Wei, Y. Xie, Y. D. Xing, L. C. Wang, H. Q. Ye, X. Xiong, S. Wang, K. Han, *J. Membr. Sci.* **2019**, *582*, 414.
- [14] L. Ding, L. B. Li, Y. C. Liu, Y. Wu, Z. Lu, J. J. Deng, Y. Y. Wei, J. Caro, H. H. Wang, *Nat. Sustain.* **2020**, *3*, 296.
- [15] a) S. W. Shi, B. Q. Qian, X. Y. Wu, H. L. Sun, H. Q. Wang, H. B. Zhang, Z. Z. Yu, T. P. Russell, *Angew. Chem., Int. Ed.* **2019**, *58*, 18171; b) X. P. Li, X. F. Li, H. G. Li, Y. Zhao, J. Wu, S. K. Yan, Z. Z. Yu, *Adv. Funct. Mater.* **2021**, 2110636.
- [16] Z. Li, Y. Wei, X. Gao, L. Ding, Z. Lu, J. Deng, X. Yang, J. Caro, H. Wang, *Angew. Chem., Int. Ed.* **2020**, *59*, 9751.
- [17] M. Ghidui, M. R. Lukatskaya, M. Q. Zhao, Y. Gogotsi, M. W. Barsoum, *Nature* **2014**, *516*, 78.
- [18] L. Ding, Y. Y. Wei, L. B. Li, T. Zhang, H. H. Wang, J. Xue, L. X. Ding, S. Q. Wang, J. Caro, Y. Gogotsi, *Nat. Commun.* **2018**, *9*, 155.
- [19] Z. Lu, Y. Y. Wei, J. J. Deng, L. Ding, Z. K. Li, H. H. Wang, *ACS Nano* **2019**, *13*, 10535.
- [20] G. Z. Liu, J. Shen, Y. F. Ji, Q. Liu, G. P. Liu, J. Yang, W. Q. Jin, *J. Mater. Chem. A* **2019**, *7*, 12095.
- [21] a) J. Wang, Z. J. Zhang, J. N. Zhu, M. T. Tian, S. C. Zheng, F. D. Wang, X. D. Wang, L. Wang, *Nat. Commun.* **2020**, *11*, 3540; b) Y. Y. Fan, L. Y. Wei, X. X. Meng, W. M. Zhang, N. T. Yang, Y. Jin, X. B. Wang, M. W. Zhao, S. M. Liu, *J. Membr. Sci.* **2019**, *569*, 117.
- [22] Q. W. Long, S. F. Zhao, J. X. Chen, Z. Zhang, G. X. Qi, Z. Q. Liu, *J. Membr. Sci.* **2021**, *635*, 119464.
- [23] a) J. N. Zhu, L. Wang, J. Wang, F. D. Wang, M. T. Tian, S. C. Zheng, N. Shao, L. L. Wang, M. He, *ACS Nano* **2020**, *14*, 15306; b) Y. Sun, S. Li, Y. Zhuang, G. Liu, W. Xing, W. Jing, *J. Membr. Sci.* **2019**, *591*, 117350; c) J. J. Deng, Z. Lu, L. Ding, Z. K. Li, Y. Y. Wei, J. Caro, H. H. Wang, *Chem. Eng. J.* **2021**, *408*, 127806.
- [24] L. Cao, P. C. Dai, J. Tang, D. Li, R. H. Chen, D. D. Liu, X. Gu, L. J. Li, Y. Bando, Y. S. Ok, X. B. Zhao, Y. Yamauchi, *J. Am. Chem. Soc.* **2020**, *142*, 8755.
- [25] a) X. L. Wu, X. L. Cui, W. J. Wu, J. T. Wang, Y. F. Li, Z. Y. Jiang, *Angew. Chem., Int. Ed.* **2019**, *58*, 18524; b) N. Wang, G. Yang, H. X. Wang, C. Z. Yan, R. Sun, C. P. Wong, *Mater. Today* **2019**, *27*, 33; c) S. Zhang, W. Chen, Y. Zhao, K. Yang, B. Du, L. Ding, W. Yang, S. Wu, *Compos. B: Eng.* **2021**, *223*, 15; d) K. Jasuja, K. Ayinde, C. L. Wilson, S. K. Behura, M. A. Ikenbbery, D. Moore, K. Hohn, V. Berry, *ACS Nano* **2018**, *12*, 9931.
- [26] W. Eom, H. Shin, R. B. Ambade, S. H. Lee, K. H. Lee, D. J. Kang, T. H. Han, *Nat. Commun.* **2020**, *11*, 2825.
- [27] a) Z. Lu, Y. Wu, L. Ding, Y. Y. Wei, H. H. Wang, *Angew. Chem., Int. Ed.* **2021**, *60*, 22265; b) Y. Q. Sun, D. Xu, S. L. Li, L. L. Cui, Y. X. Zhuang, W. H. Xing, W. H. Jing, *J. Membr. Sci.* **2021**, *623*, 119075; c) Y. Y. Fan, J. Y. Li, S. D. Wang, X. X. Meng, W. M. Zhang, Y. Jin, N. T. Yang, X. Y. Tan, J. Q. Li, S. M. Liu, *Chem. Eng. J.* **2020**, *401*, 126073.
- [28] F. M. Guo, X. Shen, J. M. Zhou, D. Liu, Q. B. Zheng, J. L. Yang, B. H. Jia, A. K. T. Lau, J. K. Kim, *Adv. Funct. Mater.* **2020**, *30*, 1910826.
- [29] a) H. A. Lee, Y. F. Ma, F. Zhou, S. Hong, H. Lee, *Acc. Chem. Res.* **2019**, *52*, 704; b) H. A. Lee, E. Park, H. Lee, *Adv. Mater.* **2020**, *32*, 8319. c) P. Yang, F. Zhu, Z. B. Zhang, Y. Y. Cheng, Z. Wang, Y. W. Li, *Chem. Soc. Rev.* **2021**, *50*, 8319.
- [30] J. Li, L. Li, Y. L. Xu, J. Y. Zhu, F. Liu, J. N. Shen, Z. Y. Wang, J. Y. Lin, *Chem. Eng. J.* **2022**, *427*, 132070.
- [31] a) Y. Lv, C. Zhang, A. He, S. J. Yang, G. P. Wu, S. B. Darling, Z. K. Xu, *Adv. Funct. Mater.* **2017**, *27*, 1700251; b) W. Y. Ye, K. F. Ye, F. Lin, H. W. Liu, M. Jiang, J. Wang, R. R. Liu, J. Y. Lin, *Chem. Eng. J.* **2020**, *379*, 122321; c) S. J. Yang, L. Y. Zou, C. Liu, Q. Zhong, Z. Y. Ma, J. Yang, J. Ji, P. Muller-Buschbaum, Z. K. Xu, *ACS. Appl. Mater. Interfaces.* **2020**, *12*, 59094.
- [32] a) L. Hu, S. J. Gao, X. G. Ding, D. Wang, J. Jiang, J. Jin, L. Jiang, *ACS Nano* **2015**, *5*, 4835; b) Y. Z. Zhu, W. Xie, S. J. Gao, F. Zhang, W. B. Zhang, Z. Y. Liu, J. Jin, *Small* **2016**, *12*, 5034.
- [33] a) J. D. Wu, W. Wei, S. H. Li, Q. Zhong, F. Liu, J. H. Zheng, J. P. Wang, *J. Membr. Sci.* **2018**, *563*, 126; b) J. Yang, H. N. Li, Z. X. Chen, A. He, Q. Z. Zhong, Z. K. Xu, *J. Mater. Chem. A* **2019**, *7*, 7907; c) Y. F. Wang, Z. L. Liu, X. C. Wei, K. L. Liu, J. H. Wang, J. T. Hu, J. Lin, *Chem. Eng. J.* **2021**, *413*, 127493; d) C. H. Liu, J. Y. Xia, J. C. Gu, W. Q. Wang, Q. Q. Liu, L. K. Yan, T. Chen, *J. Hazard. Mater.* **2021**, *403*, 123547.